Applied Catalysis B: Environmental 152–153 (2014) 335–341

Contents lists available at ScienceDirect

Applied Catalysis B: Environmental

journal homepage: www.elsevier.com/locate/apcatb

In-situ reduction synthesis of nano-sized Cu_2O particles modifying g-C_3N_4 for enhanced photocatalytic hydrogen production

Jie Chen, Shaohua Shen*, Penghui Guo, Meng Wang, Po Wu, Xixi Wang, Liejin Guo*

International Research Centre for Renewable Energy, State Key Laboratory of Multiphase Flow in Power Engineering, Xi'an Jiaotong University, Xi'an 710049, Shaanxi, China

ARTICLE INFO

Article history:
Received 10 November 2013
Received in revised form 21 January 2014
Accepted 26 January 2014
Available online 2 February 2014

Keywords:
Cu_2O/g-C_3N_4
Type II band alignment
Hydrogen production
Photocatalytic

ABSTRACT

Cu_2O nanoparticles (NPs) were directly formed on g-C_3N_4 via a one-pot in-situ reduction method. The physical and photophysical properties of these Cu_2O NPs modified g-C_3N_4 photocatalysts were characterized to investigate the effects of Cu_2O NPs on the photocatalytic activities of g-C_3N_4. Close contact was formed between Cu_2O and g-C_3N_4 and the Cu_2O NPs were well dispersed on g-C_3N_4. The visible light photocatalytic hydrogen production activity over g-C_3N_4 was enhanced by more than 70% with Cu_2O NPs modification. It is revealed that the efficient visible light absorption and Type II band alignment induced charge separation by Cu_2O NPs modification should be the key factors for improved photocatalytic performance.

© 2014 Elsevier B.V. All rights reserved.

1. Introduction

Photocatalytic water splitting to produce hydrogen has attracted great research interest due to the global energy crisis and environmental pollution since its first demonstration by Fujishima and Honda [1]. During the past few decades, many photocatalysts have been developed, such as TiO_2, [2] CdS [3], etc. However, various drawbacks, such as poor absorption ability (e.g. TiO_2) [2], fast recombination rate of photogenerated electron–hole pairs, and highly toxic for human health and harmful to the environment (e.g. CdS) [3] greatly limit the photocatalytic efficiency and practical application for solar hydrogen conversion. To address these limitations, novel photocatalytic materials of efficient visible light absorption and charge separation must be developed for practical application of this state-of-the-art technique for solar fuel production.

Recently, Wang et al. [4,5] reported a novel metal-free polymer n-type semiconductor, layered C_3N_4 with a graphitic structure (g-C_3N_4), showing good visible light absorption property (E_g = 2.7 eV) and photocatalytic stability for hydrogen production. Compared with the most studied materials (TiO_2, CdS, etc.), g-C_3N_4 combines the advantages of low cost, nontoxicity and visible light activity, and in this regard, it should be a good candidate for photocatalytic solar conversion. However, the photocatalytic efficiency of pure g-C_3N_4 was relatively low, mainly due to the fast recombination of photogenerated electron–hole pairs. By far, two approaches have been considered effective to increase the separation efficiency of photogenerated electron–hole pairs for g-C_3N_4. One is to load co-catalysts, such as Au, Pt and Ag, on the surface of catalysts [6–8]. For example, Maeda et al. found that Pt loading could greatly improve the visible light photocatalytic hydrogen production performance for g-C_3N_4 [6], and they further loaded Au, Pt, Pd on g-C_3N_4 and found that compared with Pt loading alone, the photocatalytic hydrogen production ability was enhanced by more than 5 times with Au, Pt coloading [7].

The other way is to form semiconductor heterojunctions with properly aligned band structure [9,10]. Coupling with quantum dots (QDs) of narrow band gap semiconductors has been proven to be effective to improve photoactivity of g-C_3N_4 in the visible spectrum. Ge et al. [11] reported a novel CdS QDs modified g-C_3N_4 photocatalyst with efficient separation of the photogenerated charge carriers and thus enhanced visible light photocatalytic hydrogen production activity. Different QDs, such as CdSe [12], and Cu_2O [13,14] have been coupled with other photocatalysts for better activity. Tennakone et al. [13] developed Cu_2O QDs modified TiO_2 nanoparticles for enhanced photocatalytic activity for water photoreduction by promoting inter-particle charge transfer to suppress charge carrier recombination. Lin et al. [14] reported

* Corresponding authors. Xi'an Jiaotong University, International Research Centre for Renewable Energy, State Key Laboratory of Multiphase Flow in Power Engineering, Xianning West Road 28#, Xi'an 710049, Shaanxi, China. Tel.: +86 29 8266 8296; fax: +86 29 8266 9033.
E-mail addresses: shshen_xjtu@mail.xjtu.edu.cn (S. Shen), lj-guo@mail.xjtu.edu.cn (L. Guo).

0926-3373/$ – see front matter © 2014 Elsevier B.V. All rights reserved.
http://dx.doi.org/10.1016/j.apcatb.2014.01.047

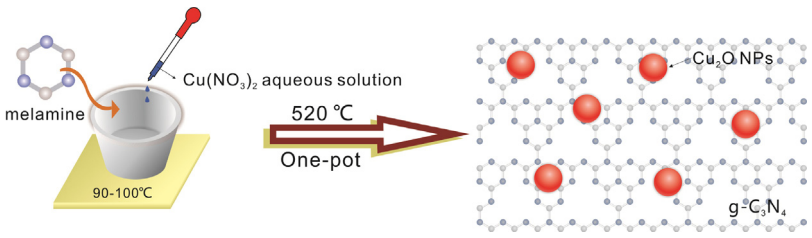

Fig. 1. Schematic illustration of the fabrication of Cu_2O NPs/g-C_3N_4 composite photocatalysts.

Cu_2O/TiO_2 p–n heterojunction composed of Cu_2O nanoparticles deposited on TiO_2 and the visible light photocatalytic for degrading RhB was significantly enhanced due to broadened absorption in the visible light region and improved separation of photogenerated electrons and holes. However, nowadays, in most studies on Cu_2O modification, cumbersome two-step method was used for sample preparation and the Cu_2O particles were easy to be oxidized [15] for exposure to air during the synthesis process. To our best knowledge, there is still rare report on nano-sized Cu_2O particles modified g-C_3N_4 photocatalyst prepared by a facile one-pot method for improved hydrogen production activity under visible light.

In the present study, we successfully prepared a series of Cu_2O NPs modified g-C_3N_4 photocatalysts via a one-pot in-situ reduction method. The effects of Cu_2O NPs on the visible optical absorption and charge carrier separation, and hence the photocatalytic activities of g-C_3N_4 were discussed in detail.

2. Experimental

2.1. Synthesis procedure

All chemicals in the present study are of analytical grade and used as received without further purification. Cu_2O NPs modified g-C_3N_4 photocatalysts were prepared as illustrated in Fig. 1. Typically, 5.0 g melamine and desired volume of 0.0760 g/mL $Cu(NO_3)_2{\cdot}3H_2O$ aqueous solution (typically, 1.0 mL of $Cu(NO_3)_2{\cdot}3H_2O$ aqueous solution resulting in 1.0 wt% of Cu in the as-prepared Cu_2O/g-C_3N_4 photocatalyst) were added into 200 mL distilled water. The obtained solution was heated at 90 °C for 1 h under stirring, then the temperature was raised to 100 °C for complete water evaporation. The resulting mixture was put into an alumina crucible with a cover, and heated to 520 °C with ramping rate of 20 °C/min and kept at that temperature for another 4 h. This process was conducted with 30 mL/min N_2 flow at atmospheric pressure. g-C_3N_4 modified with different amounts of Cu_2O NPs is denoted as Cu(*X* wt%)-g-C_3N_4, where *X*, ranging from 0 to 1.0, is used to note the Cu content in the as-prepared Cu_2O/g-C_3N_4 photocatalyst.

Pure g-C_3N_4 was prepared by the same process without adding $Cu(NO_3)_2$. Pure Cu_2O powders were obtained by completely decomposing g-C_3N_4 in Cu(1.0 wt%)-g-C_3N_4 under 800 °C for 2 h at N_2 atmosphere. Cu_2O/g-C_3N_4-M composite as reference was prepared by mechanical mixing of pure Cu_2O and pure g-C_3N_4.

2.2. Characterization

The transmission electron microscopy (TEM) images were obtained from a FEI Tecnai G2 F30 transmission electron microscope at an accelerating voltage of 300 kV. The X-ray diffraction (XRD) patterns were obtained from a PANalytical X'pert MPD Pro diffractometer operated at 40 kV and 40 mA using Ni-filtered Cu *K*α irradiation (Wavelength 1.5406 Å). UV–vis absorption spectra (UV–vis) were measured on a HITACHI U4100 instrument equipped with labsphere diffuse reflectance accessory. The analysis of photoluminescence spectra (PL) was carried out at room temperature on a PTI QM-4 fluorescence spectrophotometer. X-ray photoelectron spectroscopy (XPS) data were obtained on a Kratos Axis-Ultra DLD instrument with a monochromatized Al *K*α line source (150 W). All binding energies were referenced to the C 1s peak at 284.8 eV.

2.3. Photocatalytic activity evaluation

Photocatalytic hydrogen evolution was performed in a gas-closed circulation system with an approximate 230 mL top window Pyrex cell as the photoreactor. A 300 W Xe lamp was used as the light source, and the UV part of the light was removed by a cutoff filter ($\lambda > 420$ nm). Hydrogen evolved was analyzed on a thermal conductivity detector (TCD) gas chromatograph (NaX zeolite column, N_2 as a carrier gas) every 60 min. In a typical experiment, the photocatalyst powder (0.1 g) was dispersed in 180 mL of 10 vol% triethanolamine (TEOA) aqueous solution under stirring. Pt (3 wt%) was photodeposited in situ on the photocatalysts from the precursor of $H_2PtCl_6{\cdot}6H_2O$. Nitrogen was purged through the cell for 15 min before photocatalytic reaction to remove oxygen. The temperature for all the photocatalytic reactions was kept at 35 ± 0.5 °C by thermostatic waterbath.

3. Results and discussion

3.1. Structure and morphology

The TEM images of the as-prepared Cu(*X* = 0, 0.05, 0.5, 1.0 wt%)-g-C_3N_4 photocatalysts are shown in Fig. 2. Fig. 2A is the TEM image of the pure g-C_3N_4 photocatalyst, showing a layered structure, which offers substrate for loading of Cu_2O NPs. For the modified samples (Fig. 2B–E), Cu_2O NPs are well dispersed on g-C_3N_4. The fringes spacing measured to be 2.46 Å and 2.13 Å were corresponded to (2 1 1) and (2 0 0) lattice plane of cuprite Cu_2O (JCPDS 005-0667), respectively. As demonstrated in Fig. 2B, for the Cu(0.05 wt%)-g-C_3N_4 photocatalyst, Cu_2O NPs were dispersed evenly on g-C_3N_4 with a narrow size range of 3–7 nm. While *X* increasing to more than 0.5, larger particles appeared for Cu(0.5 wt%)-g-C_3N_4 and Cu(1.0 wt%)-g-C_3N_4 sample (Fig. 2C and D). The particle size distribution (Fig. 2F) was recorded by measuring more than 60 nanoparticles from TEM images for Cu(0.05 wt%)-g-C_3N_4 and Cu(0.5 wt%)-g-C_3N_4. The diameters of Cu_2O NPs in Cu(0.05 wt%)-g-C_3N_4 are centered at 4 nm. For Cu(0.5 wt%)-g-C_3N_4, the size distribution of Cu_2O NPs turns to be wider, and larger particles with diameter >10 nm or small particles with diameter <3 nm can be also found. Further increasing the amount of $Cu(NO_3)_2$ precursor gives rise to more nanoparticles with larger size up to ~18 nm, as observed for Cu(1.0 wt%)-g-C_3N_4 (Fig. 2E).

The XRD patterns of the Cu(*X* wt%)-g-C_3N_4 samples are presented in Fig. 3 to investigate the structure of g-C_3N_4 after modifying with Cu_2O NPs. All the samples show quite similar profiles and all the diffraction peaks can be attributed to the

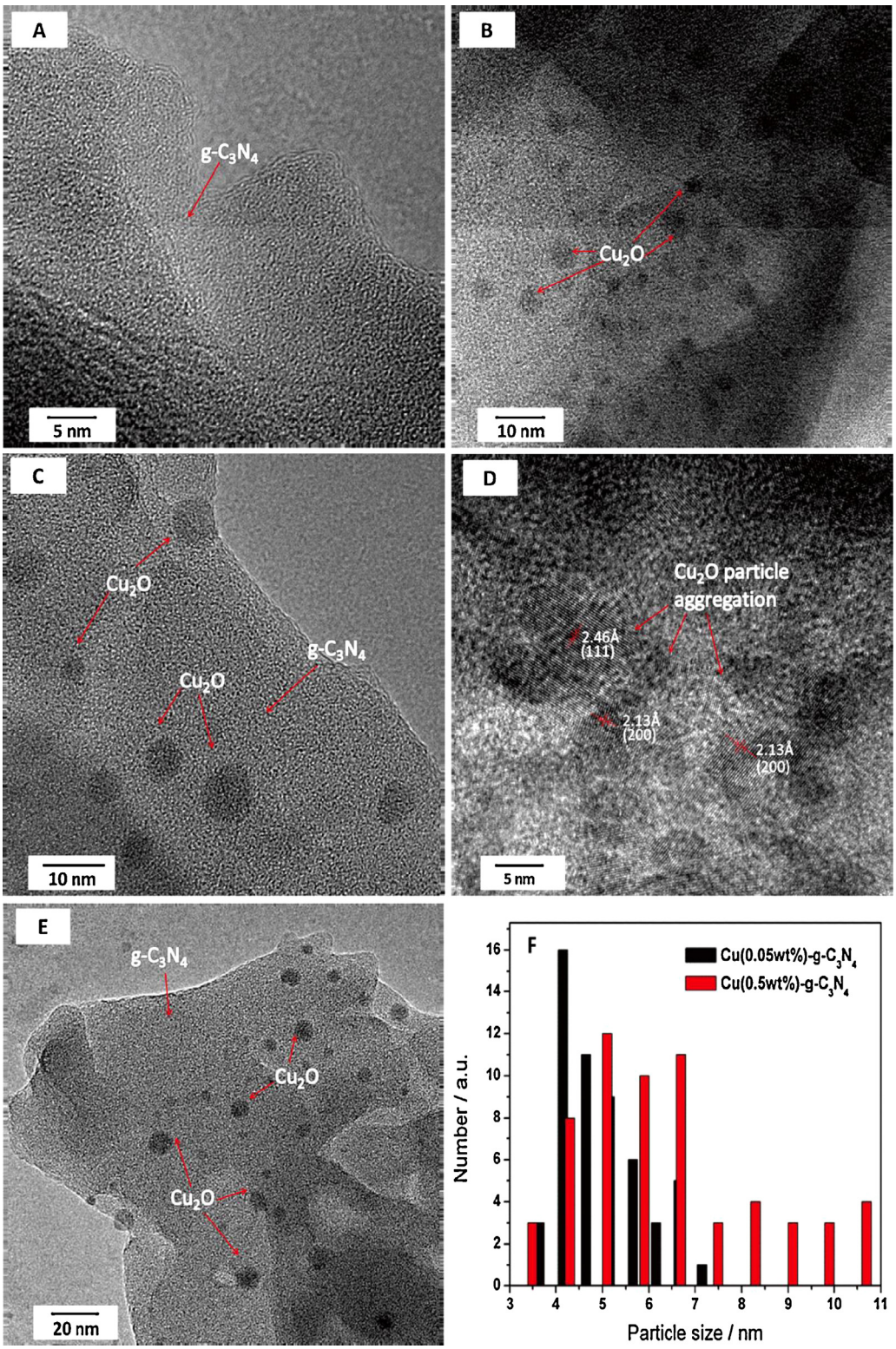

Fig. 2. TEM images of Cu(X wt%)-g-C_3N_4 photocatalysts: (A) X = 0; (B) X = 0.05; (C and D) X = 0.5; (E) X = 1.0; (F) the particle size distribution for Cu(X = 0.05, 0.5 wt%)-g-C_3N_4.

graphitic phase with tri-*s*-triazine unit in its structure [4,16]. The unchanged peak position and shape indicates that the g-C_3N_4 nanolayer structure does not change with Cu_2O modification. No Cu_2O peaks were detected from the XRD patterns, mainly because the nanoparticles in those samples are well dispersed at several nanometer scale (as seen in Fig. 1) and the Cu_2O contents are quite low [17,18].

3.2. Chemical state of Cu

To confirm the chemical state of Cu in these photocatalysts, Cu 2p XPS spectra of Cu(X wt%)-g-C_3N_4 were analyzed, as shown in Fig. 4. The peaks at 932.4 eV and 952.1 eV are attributed to Cu^{2+} ions according to the previous reports [15,19,20]. The Cu $2p_{3/2}$ level shifted a little toward lower binding energy compared to

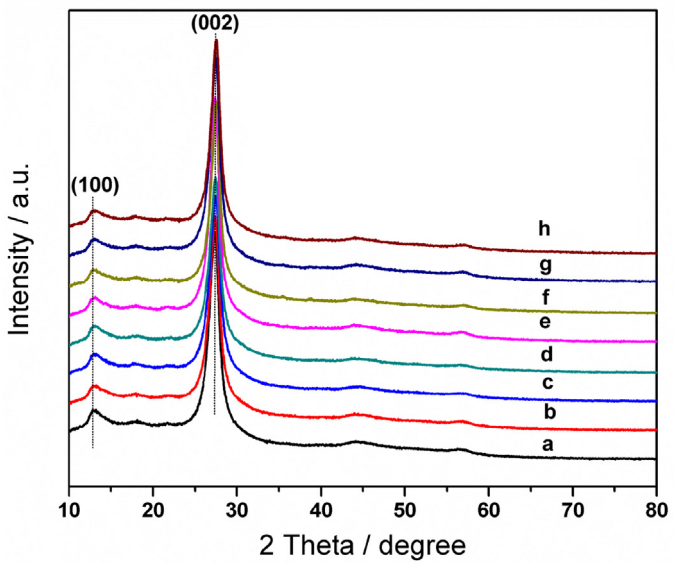

Fig. 3. X-ray diffraction patterns of Cu(X wt%)-g-C_3N_4 photocatalysts with various X: (a) X = 1.0; (b) X = 0.7; (c) X = 0.5; (d) X = 0.2; (e) X = 0.1; (f) X = 0.05; (g) X = 0.02; (h) X = 0.

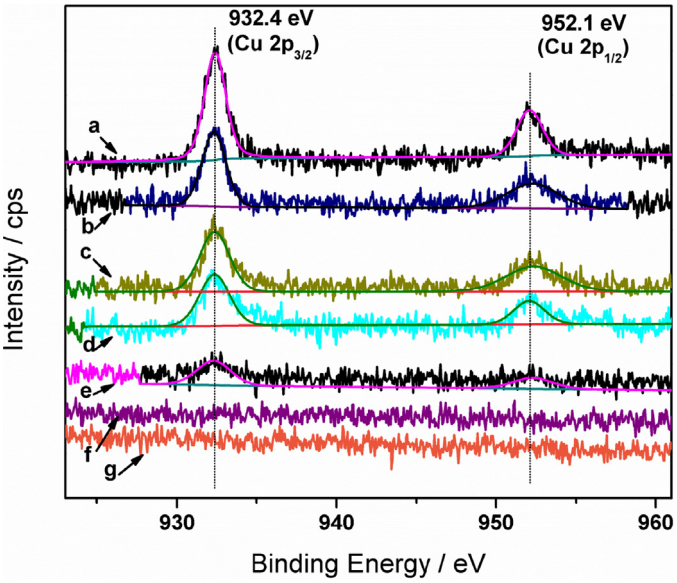

Fig. 4. Cu 2p XPS spectra of the Cu(X wt%)-g-C_3N_4 photocatalysts with various X: (a) X = 1.0; (b) X = 0.7; (c) X = 0.5; (d) X = 0.2; (e) X = 0.1; (f) X = 0.05; (g) X = 0.02.

that of bulk Cu_2O (932.6 eV) [20], indicating that the formed Cu_2O species on g-C_3N_4 existed as nanocrystallines or quantum dots [15]. No satellite peaks around 945.0 eV, characteristic of the Cu^{2+} ions [21–23], were detected. The increasing intensity of Cu 2p peaks should be due to the increased content of Cu_2O. As confirmed by XPS quantitative analysis, the amounts of Cu for the Cu(X = 0.1, 0.2, 0.5, 0.7, 1.0 wt%)-g-C_3N_4 samples were calculated to be 0.09 wt%, 0.22 wt%, 0.47 wt%, 0.66 wt% and 0.94 wt%, respectively, which are very close to the value of initial Cu content. The XPS spectra of Cu 2p were undetectable when Cu content was smaller than 0.1 wt%, possibly due to the detection limit of XPS instrument.

3.3. Optical properties

Fig. 5 shows the UV–vis diffuse reflectance spectra of the as-prepared photocatalysts. The absorption edge of pure g-C_3N_4 photocatalysts was about 460 nm, with band gap (E_g) calculated to be 2.70 eV by Kubelka–Munk method [24]. The absorption edge monotonously red-shifted from 460 nm for g-C_3N_4 to 600 nm for Cu(1.0 wt%)-g-C_3N_4 with increasing Cu_2O loading amounts. The broadening of light absorption may be attributed to the loaded Cu_2O known as a p-type semiconductor oxide with E_g of 2.0–2.4 eV, depending on the nanoparticle size [25,26]. As shown in Fig. 5, the light absorption edge of pure Cu_2O with particle size of 30 nm (Fig. S1–S2) is 630 nm, corresponds to a band gap of 1.97 eV, which is in accord with the reported value [25,26]. It has also been reported that for Cu_2O NPs with size of about 2–3 nm, the band gap might increase to 2.40 eV due to quantum size effect [25,26].

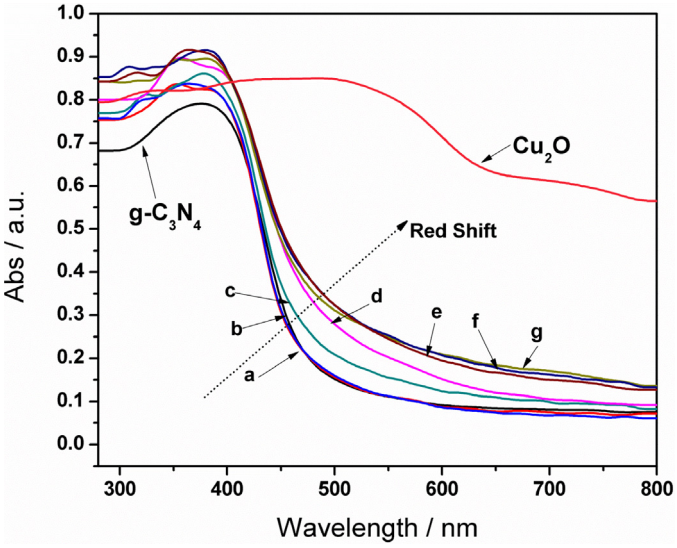

Fig. 5. UV–vis diffuse reflectance spectra of pure g-C_3N_4, pure Cu_2O and Cu(X wt%)-g-C_3N_4 photocatalysts with various X: (a) X = 0.02; (b) X = 0.05; (c) X = 0.1; (d) X = 0.2; (e) X = 0.5; (f) X = 0.7; (g) X = 1.0.

Photoluminescence (PL) spectroscopy has been widely used to examine the charge transfer, migration and separation in photocatalysts [27]. Fig. 6 shows the PL spectra for pure g-C_3N_4 as well as Cu(X wt%)-g-C_3N_4. All the photocatalysts exhibited a broad emission peak centered at around 460 nm, corresponding to the band gap of g-C_3N_4, and a tail extending to 650 nm. The emission could be attributed to the band–band PL phenomenon of the photoinduced charge carriers for g-C_3N_4 [5,9]. The PL

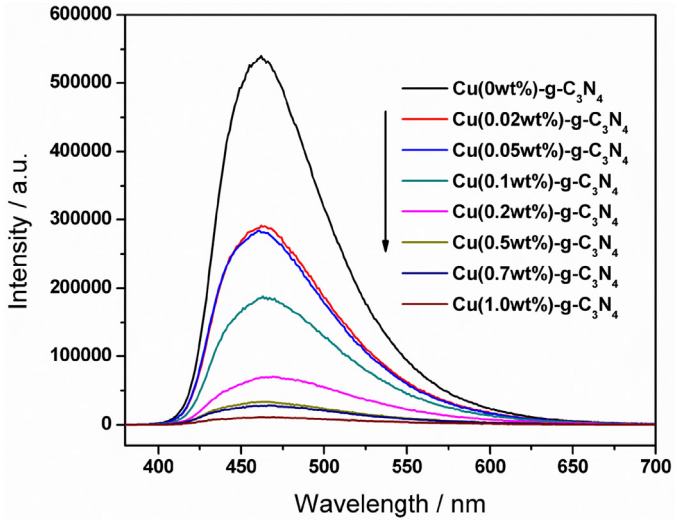

Fig. 6. Photoluminescence spectra of Cu(X wt%)-g-C_3N_4 photocatalysts.

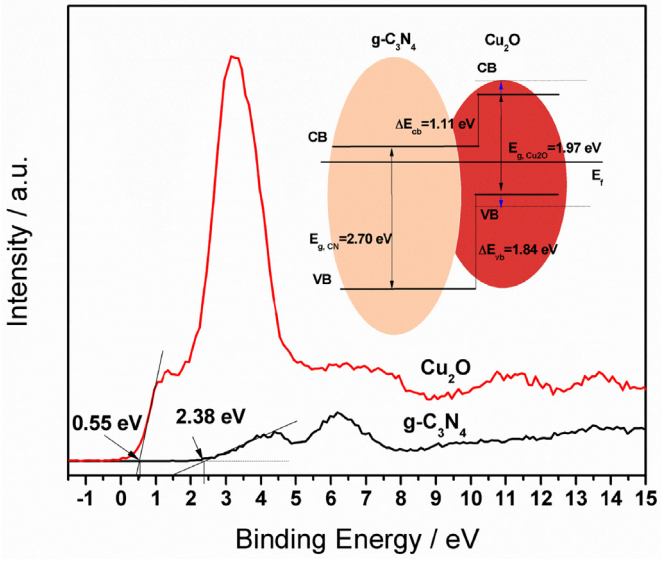

Fig. 7. VB XPS spectra for Cu_2O and g-C_3N_4. The inset is the energy band alignment of Cu_2O/g-C_3N_4 heterojunction. (solid lines: band position for pure Cu_2O and g-C_3N_4; dotted lines: estimated band position for Cu_2O nanoparticles).

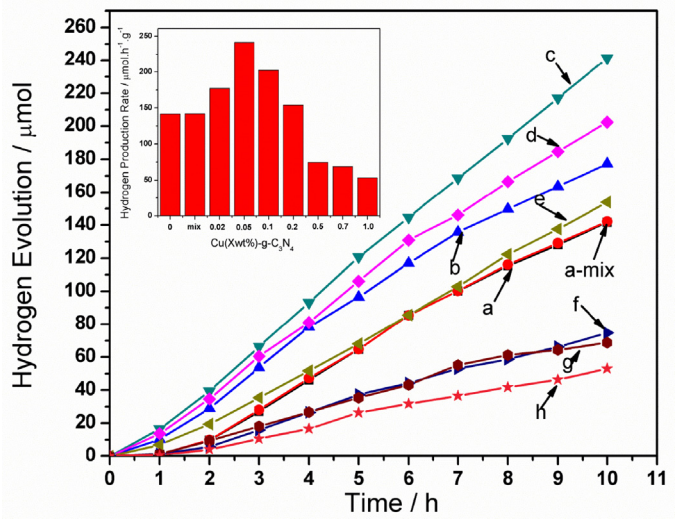

Fig. 8. Photocatalytic H_2 production under visible-light irradiation over Cu(X wt%)-g-C_3N_4 photocatalysts: (a) X = 0; (b) X = 0.02; (c) X = 0.05; (d) X = 0.1; (e) X = 0.2; (f) X = 0.5; (g) X = 0.7; (h) X = 1.0; a-mix: Cu_2O/g-C_3N_4-M, mechanical mixture of Cu_2O and g-C_3N_4 with Cu content of 0.05 wt%.

emission intensity exhibits the highest value for the pure g-C_3N_4 and decreases monotonously with increasing Cu_2O contents. This indicates that the recombination of photogenerated charge carriers is inhibited in the Cu(X wt%)-g-C_3N_4 photocatalysts. The charge separation in composite photocatalysts is usually attributed to the charge transfer at the interfaces, with driving force originated from the matching band potentials of the two components (e.g. type II band alignment) [28].

3.4. Band alignment

In the present work, the valence band maximum (VBM) edge potentials of Cu_2O and g-C_3N_4 was measured by the valence band X-ray photoelectron spectroscopy (VB XPS) to demonstrate the band alignment occurred for the Cu(X wt%)-g-C_3N_4 photocatalysts. As shown in Fig. 7, the VBM energy levels of Cu_2O and g-C_3N_4 were determined to be about 0.55 eV and 2.38 eV, respectively. The valence band offset (VBO, ΔE_{vb}) and the conduction band offset (CBO, ΔE_{cb}) are described by the following formula, [29,30] which is considered accurate in determining the band offset of heterojunction structure:

$$\Delta E_{vb}(C_3N_4/Cu_2O) = (E_{N1s,\,C_3N_4} - E_{VBM,\,C_3N_4}) - (E_{Cu\ 2p_{3/2},\,Cu_2O} - E_{VBM,\,Cu_2O}) + (E_{Cu\ 2p_{3/2},\,interface} - EN\ 1s,\,interface) \quad (1)$$

$$\Delta E_{cb}\left(\frac{C_3N_4}{Cu_2O}\right) = (E_{g,C_3N_4} - E_{g,Cu_2O}) - \Delta E_{vb}\left(\frac{C_3N_4}{Cu_2O}\right) \quad (2)$$

where $(E_{Cu\ 2p_{3/2},\ interface} - E_{N\ 1s,\ interface})$ is the energy difference between Cu $2p_{3/2}$ and N 1s core levels (Fig. S3), which measured in the Cu_2O/g-C_3N_4 heterojunction, $(E_{N\ 1s,\ C_3N_4} - E_{VBM,\ C_3N_4})$ and $(E_{Cu\ 2p_{3/2},\ Cu_2O} - E_{VBM,\ Cu_2O})$ are the g-C_3N_4 and Cu_2O constants, which are obtained from each pure component. Note that the E_g and VBM position were measured from pure Cu_2O made by decomposing g-C_3N_4 in Cu_2O/g-C_3N_4 to estimate the real E_g and VBM values of the loaded Cu_2O NPs in the present work. Indeed, the real E_g value for the quantum-sized Cu_2O NPs in the as-prepared g-C_3N_4/Cu_2O composite photocatalysts must be larger (dotted line in Fig. 7), as previously reported that the VB and CB position should oppositely separate due to the quantum size effect [14]. Based on the above deduction, as illustrated in Fig. 7, Cu_2O displays a CB energy level 1.11 eV higher than g-C_3N_4, indicating that the photoelectrons can transfer from Cu_2O nanoparticles easily to g-C_3N_4. Meanwhile, the photoinduced holes on the g-C_3N_4 surface can move to Cu_2O due to the 1.84 eV VBM energy level difference between the two components. Thus, the possibility for the electron–hole recombination could be greatly reduced by charge carrier transfer between g-C_3N_4 and Cu_2O induced by proper Type II band alignment.

3.5. Photocatalytic performance for hydrogen production

The photocatalytic activity of Cu(X wt%)-g-C_3N_4 was evaluated by hydrogen production reaction under visible light ($\lambda > 420$ nm), as shown in Fig. 8. All the samples are photocatalytically active and stable for hydrogen production. No hydrogen was detected in the absence of either photocatalyst or light irradiation. The rate of hydrogen evolution over pure g-C_3N_4 was 141.6 μmol/h/g. With Cu_2O contents increasing, the photocatalytic activity was improved, with the highest activity obtained for X = 0.05, and the hydrogen evolution rate achieved 241.3 μmol/h/g. However, the photocatalytic activity was decreased with the further increasing of loading contents of Cu_2O for Cu(X wt%)-g-C_3N_4 (X = 0.1–1.0).

To clarify the photocatalytic hydrogen production reaction mechanism, we must make it clear that the Cu_2O NPs influenced the activity of g-C_3N_4 via three effects: (1) efficient charge separation induced by the Type II band alignment; (2) acting as visible light sensitizers; (3) the negative shading effect [14,31]. The shading effect implied that more $Cu(NO_3)_2$ addition will lead to the formation of much larger Cu_2O NPs covering on the surface of g-C_3N_4 and then reduce the numbers of g-C_3N_4 active sites available for H_2 production. Note that effect (2) and (3) were both related to the Cu_2O content, that is, the larger the content, the stronger the effects of both (2) and (3). As shown from the UV–vis diffuse reflectance spectra in Fig. 5, the optical absorption of these photocatalysts were improved due to Cu_2O NPs modification, given the Type II band alignment, it was possible for the photoexcited electrons in Cu_2O NPs to transfer to g-C_3N_4, in other words, the Cu_2O NPs could act as visible light sensitizers. However, for Cu(X wt%)-g-C_3N_4 (X = 0.02, 0.05), the amounts of Cu_2O were too small to cause

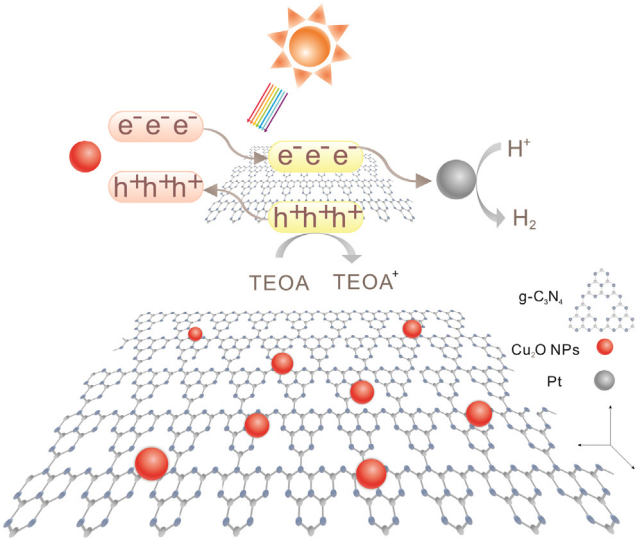

Fig. 9. Schematic of band structure and charge transfer process in Cu_2O NPs/g-C_3N_4 for photocatalytic hydrogen generation.

obvious light absorption improvement or obvious shading effect, then the photocatalytic activity improvement should be mainly due to the efficient charge separation induced by the Type II band alignment. For larger amounts of Cu_2O NPs loading (X = 0.1–1.0), although the light absorption ability was further improved, the negative shading effect turned much worse, which might greatly offset the effects of (1) and (2) and was detrimental for photocatalytic hydrogen production reaction.

Hydrogen production over mechanical mixture of Cu_2O/g-C_3N_4-M composite as reference was also tested. By comparison to Cu(0.05 wt%)-g-C_3N_4, the reference sample of Cu_2O/g-C_3N_4-M composite shows much lower photocatalytic activity under visible light, with hydrogen production rate to be only 142.0 μmol/h/g. This result indicates that the one-pot in-situ reduction method favors the formation of Cu_2O/g-C_3N_4 p–n heterojunction with intimate surface contact, and consequently resulting in efficient charge carrier separation between the two components, as illustrated in Fig. 9. The formation mechanism of the Cu_2O NPs on g-C_3N_4 is still not very clear and needs further investigation, but it is preliminarily considered that the reduction of Cu^{2+} to Cu^{+} is relevant to the reducing NH_3 atmosphere created by the deammonation process (Fig. S4), through which melamine is thermal-condensed to g-C_3N_4 [8]. Besides, the well mixture of Cu^{2+} ions and melamine molecules in the precursor aqueous solution might favor the intimate contact between Cu_2O and g-C_3N_4 and consequently the formation of p–n heterjunction.

It was reported that Cu_2O is not stable for photocatalytic reaction, due to the easy reduction and oxidation of Cu^{+} to Cu^{0} and Cu^{2+}, respectively [32]. In order to investigate the photocatalytic stability, the photocatalytic experiment was run for 5 cycles. As shown in Fig. S5 in Supplementary Information, Cu(0.05 wt%)-g-C_3N_4 shows quite good stability for photocatalytic hydrogen production during the 35 h reaction, with hydrogen production rate kept at ~241.3 μmol/h/g. The almost unchanged Cu 2p XPS spectra of Cu(1.0 wt%)-g-C_3N_4 after 5-cycle photocatalytic test (Fig. S6, Supplementary Information) further evidences the good stability of Cu(1.0 wt%)-g-C_3N_4, without changing the chemical states of Cu^{+}.

4. Conclusions

Cu_2O NPs modified g-C_3N_4 photocatalysts with varied Cu_2O contents were successfully prepared via a one-pot in-situ reduction method, which favored the formation of p–n heterojunction between Cu_2O and g-C_3N_4. As a result, the photocatalytic activity for hydrogen production over g-C_3N_4 under visible light was greatly improved by Cu_2O NPs modification. The hydrogen evolution rate was improved from 141.6 μmol/h/g (pure g-C_3N_4) to 241.3 μmol/h/g (Cu(0.05 wt%)-g-C_3N_4) by photoactivity enhancement up to ~70%. It was believed that the Cu_2O NPs could act as sensitizers for improved visible light absorption and the formed p–n heterojunction led to efficient charge separation induced by the Type II band alignment.

Acknowledgments

The authors gratefully acknowledge the financial supports from the National Natural Science Foundation of China (No. 51102194, No. 51323011, No. 51121092) and the Nano Research Program of Suzhou City (ZXG2013003). One of the authors (S. Shen) was supported by the Foundation for the Author of National Excellent Doctoral Dissertation of China (No. 201335) and the "Fundamental Research Funds for the Central Universities."

Appendix A. Supplementary data

Supplementary data associated with this article can be found, in the online version, at http://dx.doi.org/10.1016/j.apcatb.2014.01.047.

References

[1] A. Fujishima, K. Honda, Nature 238 (1972) 37–38.
[2] X.B. Chen, S.S. Mao, Chemical Reviews 107 (2007) 2891–2959.
[3] X.B. Chen, S.H. Shen, L.J. Guo, S.S. Mao, Chemical Reviews 110 (2010) 6503–6570.
[4] X.C. Wang, K. Maeda, A. Thomas, K. Takanabe, G. Xin, J.M. Carlsson, K. Domen, M. Antonietti, Nature Materials 8 (2008) 76–80.
[5] X.C. Wang, S. Blechert, M. Antonietti, ACS Catalysis 2 (2012) 1596–1606.
[6] K. Maeda, X.C. Wang, Y. Nishihara, D. Lu, M. Antonietti, K. Domen, Journal of Physical Chemistry C 113 (2009) 4940–4947.
[7] Y. Di, X.C. Wang, A. Thomas, M. Antonietti, ChemCatChem 2 (2010) 834–838.
[8] S.C. Yan, Z.S. Li, Z.G. Zou, Langmuir 25 (2009) 10397–10401.
[9] S.C. Yan, S.B. Lv, Z.S. Li, Z.G. Zou, Dalton Transactions 39 (2010) 1488–1491.
[10] Y. Wang, R. Shi, J. Lin, Y. Zhu, Energy & Environmental Science 4 (2011) 2922–2929.
[11] L. Ge, F. Zuo, J. Liu, Q. Ma, C. Wang, D.Z. Sun, L. Bartels, P.Y. Feng, Journal of Physical Chemistry C (2012) 13708–13714.
[12] J. Hensel, G. Wang, Y. Li, J.Z. Zhang, Nano Letters 10 (2010) 478–483.
[13] M.K.I. Senevirathna, P.K.D.D.P. Pitigala, K. Tennakone, Journal of Photochemistry and Photobiology A: Chemistry 171 (2005) 257–259.
[14] M.Y. Wang, L. Sun, Z.Q. Lin, J.H. Cai, K.P. Xie, C.J. Lin, Energy & Environmental Science 6 (2013) 1211–1220.
[15] Q. Sun, Y. Li, X.M. Sun, L.F. Dong, ACS Sustainable Chemistry & Engineering 1 (2013) 798–804.
[16] J.S. Zhang, J.H. Sun, K. Maeda, K. Domen, P. Liu, M. Antonietti, X.Z. Fu, X.C. Wang, Energy & Environmental Science 4 (2011) 675–678.
[17] W. Xu, X. Liu, J. Ren, P. Zhang, Y. Wang, Y.G. Guo, Y. Guo, G. Lu, Catalysis Communications 11 (2010) 721–726.
[18] Z. Zhao, X. Lin, R. Jin, Y. Dai, G. Wang, Catalysis Communications 12 (2011) 1448–1451.
[19] Y. Wu, G. Lu, S. Li, Catalysis Letters 133 (2009) 97–105.
[20] J.P. Espinós, J. Morales, A. Barranco, A. Caballero, J.P. Holgado, A.R. González-Elipe, Journal of Physical Chemistry B 106 (2002) 6921–6929.
[21] T. Ghodselahi, M.A. Vesaghi, A. Shafiekhani, A. Baghizadeh, M. Lameii, Applied Surface Science 255 (2008) 2730–2734.
[22] A. Galtayries, J.P. Bonnelle, Surface and Interface Analysis 23 (1995) 171–179.
[23] S. Poulston, P.M. Parlett, P. Stone, M. Bowker, Surface and Interface Analysis 24 (1996) 811–820.
[24] V. Kumar, S. Kr Sharma, T.P. Sharma, V. Singh, Optical Materials 12 (1999) 115–119.
[25] L. Armelao, D. Barreca, M. Bertapelle, G. Bottaro, C. Sada, E. Tondello, Thin Solid Films 442 (2003) 48–52.
[26] K. Borgohain, N. Murase, S. Mahamuni, Journal of Applied Physics 92 (2002) 1292–1297.
[27] S.H. Shen, P.H. Guo, L. Zhao, Y.C. Du, L.J. Guo, Journal of Solid State Chemistry 184 (2011) 2250–2256.
[28] J. Zhang, M. Zhang, R.Q. Sun, X.C. Wang, Angewandte Chemie International Edition 124 (2012) 10292–10296.

[29] S.C. Su, Y.M. Lu, Z.Z. Zhang, C.X. Shan, B.H. Li, D.Z. Shen, B. Yao, J.Y. Zhang, D.X. Zhao, X.W. Fan, Applied Physics Letters 93 (2008) 082108.
[30] C.H. Jia, Y.H. Chen, X.L. Zhou, A.L. Yang, G.L. Zheng, X.L. Liu, S.Y. Yang, Z.G. Wang, Applied Physics A 99 (2010) 511–514.
[31] Y.D. Hou, A.B. Laursen, J.S. Zhang, G.G. Zhang, Y.S. Zhu, X.C. Wang, S. Dahl, I. Chorkendorff, Angewandte Chemie International Edition 52 (2013) 3621–3625.
[32] P.E. de Jongh, D. Vanmaekelbergh, J.J. Kelly, Chemical Communications (1999) 1069–1070, http://pubs.rsc.org/en/content/articlelanding/1999/cc/a901232j#!divAbstract.